Research in Astronomy and Astrophysics, 26:115024 (12pp), 2026 November https://doi.org/10.1088/1674-4527/ae715f
CSTR: 32081.14.RAA.ae715f

Statistical Relationships among the Physical Properties of Dwarf Galaxies

K. Tillaboev[1,2], I. Tadjibaev[1,3], N. Otojanova[3], S. Rahimov[3], D. Otajonova[3], S. Hasanova[3,4], X. Ruzimova[3], and M. Atajonova[5]
[1] National University of Uzbekistan named after Mirzo Ulugbek, 4 University Str., Tashkent 100714, Uzbekistan ; tillaboyev_k@nuu.uz
[2] Tashkent State Medical University, Chirchik Branch, 7 Lomonosov Str., Chirchik 111718, Uzbekistan
[3] Chirchik State Pedagogical University, 104 A. Temur Str., Chirchik 111700, Uzbekistan
[4] Samarkand State Pedagogical Institute, 166 Spitamen str., Samarkand, Uzbekistan
[5] Urgench State University named after Abu Rayhon Beruni, University Str., 14 Khamid Alimjan Urgench 200100, Uzbekistan
Received 2026 March 9; revised 2026 May 3; accepted 2026 May 19; published 2026 June 16

Abstract

We present a statistical study of the global physical properties of dwarf galaxies to investigate the processes governing galaxy formation in the low-mass regime, with particular emphasis on comparing classical and Bayesian regression approaches. A unified catalog of 722 dwarf galaxies was compiled by combining structural, photometric, chemical, and dynamical data from multiple observational sources. Using Pearson, Spearman, and Kendall correlation analyses, we identify significant scaling relations among galaxy mass, luminosity, metallicity, surface brightness, size, and neutral hydrogen content, and derive both classical least-squares and Bayesian linear regressions to quantify these dependencies. We find that intrinsic relations among mass, luminosity, metallicity, surface brightness, and H I mass reflect the underlying baryonic physics within dark matter-dominated haloes. A systematic comparison shows that Bayesian regression generally yields steeper slopes for several key relations, indicating that classical methods tend to underestimate the strength of physical dependencies when measurement uncertainties and intrinsic scatter are not fully accounted for. In particular, strong mass–luminosity, mass–metallicity, and mass–surface brightness relations—further reinforced by Bayesian analysis—highlight the key role of halo mass in regulating star formation efficiency and metal retention. These trends are consistent with predictions of the Λ cold dark matter framework, where stellar feedback and gas retention processes shape the baryonic structure of low-mass galaxies. Our results provide robust empirical constraints on galaxy formation models and demonstrate the importance of Bayesian methods for accurately characterizing scaling relations, serving as a reference for testing hydrodynamical simulations and theoretical models of dark matter–baryon interactions.

Key words: catalogs – Galaxy: general – Galaxy: evolution – galaxies: dwarf – galaxies: evolution – galaxies: formation

1. Introduction

Dwarf galaxies are essential to understanding how all galaxies in the Universe form and change (Ahvazi et al. 2024; Chauhan et al. 2025). Because they are the most common type, they act as both the basic units for building larger galaxy systems and as crucial indicators of how their surroundings and internal energy processes influence them (Annibali & Tosi 2022). Their small size and simple structure make them ideal for studying the long-term effects of dark matter, stellar energy release, and the spread of heavy elements throughout cosmic history (Battaglia et al. 2008; Pontzen & Governato 2012; Sanati et al. 2023).

Within the framework of the standard Λ cold dark matter (ΛCDM) cosmological model, dwarf galaxies represent the smallest gravitationally bound systems in which galaxy formation can occur and are expected to inhabit low-mass dark matter haloes (White & Rees 1978; Springel et al. 2005). Owing to their high dark matter fractions and relatively simple baryonic structures, dwarf galaxies provide unique laboratories for probing the nature of dark matter and the efficiency of galaxy formation on small scales (Bullock & Boylan-Kolchin 2017). Their abundance, internal kinematics, and structural properties have been widely used to test ΛCDM predictions, revealing several long-standing discrepancies between theory and observations, most notably the "missing satellites" problem (Klypin et al. 1999) and the "too-big-to-fail" issue (Boylan-Kolchin et al. 2011; Vogelsberger et al. 2014).

The shallow gravitational potentials of dwarf galaxies make them especially susceptible to baryonic feedback processes such as supernova explosions, stellar winds, and radiation pressure, which can strongly regulate star formation and modify the distribution of both baryonic and dark matter components. Hydrodynamical simulations demonstrate that repeated feedback-driven gas outflows are capable of transforming the centrally concentrated dark matter cusps predicted by collisionless simulations into cored density profiles (Governato et al. 2010; Boldrini 2022; Koudmani et al. 2025; Straight et al. 2025). Consequently, dwarf galaxies are key systems for disentangling the interplay between dark matter physics and baryonic processes across cosmic time (Navarro et al. 1996; de Blok 2010; Vogelsberger et al. 2012; Zimmermann et al. 2025).

Furthermore, dwarf galaxies act as sensitive tracers of hierarchical structure formation, preserving fossil records of early star formation and chemical enrichment in the Universe. Their stellar populations, kinematics, and metallicity distributions place strong constraints on early feedback, gas accretion, and the efficiency of metal retention in low-mass systems (Bullock & Boylan-Kolchin 2017; Atek 2018; Garrison-Kimmel et al. 2019; Janz et al. 2021). Establishing robust empirical relations among the global physical properties of dwarf galaxies is therefore essential for linking observational results with theoretical models of galaxy formation within the ΛCDM paradigm (Kirby et al. 2013; Wheeler et al. 2015; Read et al. 2017).

Dwarf galaxies provide key constraints on conditions in the early Universe, as they host some of the oldest stellar populations in the nearby cosmic volume (Brown et al. 2014; Frebel & Norris 2015; Wise 2016). These ancient stars preserve chemical signatures from the epoch of reionization, offering valuable insight into early enrichment processes (Saviane et al. 2000). Owing to their low baryonic content and shallow gravitational potentials, dwarf galaxies are highly sensitive to energetic stellar feedback, including supernova explosions and stellar winds, which can regulate or even suppress star formation (Johnston et al. 1999; Behroozi et al. 2012; Leitner 2012; Koudmani et al. 2025). Recent advances enabled by facilities such as the James Webb Space Telescope (JWST), together with forthcoming surveys from the Vera C. Rubin Observatory, now allow the detection of increasingly faint dwarf systems and detailed characterization of their stellar populations (Weisz et al. 2014).

One of the earliest dwarf galaxy catalogs was compiled by van den Bergh (van den Bergh 1959) using Palomar Sky Survey data, covering objects north of -23°. It revealed a non-uniform distribution, with a concentration of dwarf irregulars near M94 in the Canes Venatici region. A later catalog of the Virgo region (Reaves 1983) included 846 dwarf galaxies over 200 square degrees, dominated by dwarf ellipticals (75%), with smaller fractions of IC 3475-type and spiral/irregular systems. Based on deep Palomar observations, it provides key structural and photometric parameters. The spatial distribution indicates that dwarf ellipticals are associated with the Virgo Cluster, while spiral and irregular dwarfs are mostly not.

A catalog of dwarf galaxies in the Fornax Cluster has been compiled, identifying 145 dwarf elliptical systems and achieving completeness down to a blue magnitude of 18.5, while also including a number of objects up to two magnitudes fainter (Caldwell 1987). In contrast to brighter cluster members, the dwarf ellipticals exhibit a less centrally concentrated spatial distribution. The relative abundance of dwarf ellipticals compared to normal ellipticals is significantly smaller in Fornax than in the Virgo Cluster. Nevertheless, the ratio of dwarf ellipticals to actively star-forming galaxies, such as spirals and irregulars, is similar in both environments. Kinematic analysis reveals that the velocity distributions of dwarf ellipticals and star-forming galaxies in Fornax depart from a Gaussian form, whereas elliptical and lenticular (E/S0) galaxies display a velocity distribution consistent with a Gaussian profile. The E/S0 population is further characterized by a comparatively low velocity dispersion of approximately $300\ \mathrm{km\ s^{-1}}$.

Dwarf galaxies in the Local Group serve as key laboratories for studying the most common galaxy type. Mateo's review (Mateo 1998) compiled extensive data on their photometry, structure, interstellar medium, chemical enrichment, star formation, and kinematics, including dark matter and interaction signatures. Although many issues raised in that work have since been addressed, some remain unresolved, and the Local Group continues to be a fundamental framework for understanding galaxy formation and evolution.

The catalog of dwarf galaxies in and around the Local Group (McConnachie 2012) summarizes their positional, structural, and kinematic properties for over 100 galaxies within 3 Mpc. It includes satellites of the Milky Way and M31, as well as isolated systems, while excluding nearby groups such as Maffei, Sculptor, and IC 342. The dataset compiles key parameters—distances, velocities, luminosities, metallicities, and structural properties—in a homogeneous form with evaluated uncertainties. It also examines the spatial structure of the Local Group, morphological diversity, evolutionary timescales, and scaling relations, including trends in metallicity and possible lower limits in surface brightness at low luminosities.

An extensive review of the Local Volume dwarf galaxy catalog (Karachentsev & Kaisina 2019) includes about 1000 systems within 11 Mpc, most of which have stellar masses $M_{*}/M_{\odot} < 10^{9}$. Around 40% have precise distance measurements from the Hubble Space Telescope. This dataset provides one of the most complete and least biased samples for testing the ΛCDM model on small scales. It includes star formation rates, H II region properties, and explores relations such as the baryonic Tully–Fisher relation, while also using dwarf galaxies as tracers of masses in nearby groups and the Virgo Cluster.

A comprehensive review of dwarf galaxies, covering their properties, formation and evolution within the ΛCDM framework, star formation histories, environmental effects, and the role of dark matter, is provided in Tillaboev et al. (2025a).

For decades, dwarf galaxy catalogs have provided key data on their properties, yet the relationships between fundamental parameters—such as stellar mass, luminosity, and size—remain unclear, especially across heterogeneous datasets. Understanding these relations is essential for galaxy formation studies. We present a compiled catalog of dwarf galaxies and analyze statistical relations between their main properties using correlation and regression methods. Our goal is to summarize these relations, test them against theory, and provide a unified dataset for future research.

2. Methods

2.1. Correlation Analysis

To quantify the relationships between the physical parameters of dwarf galaxies, we employed three complementary statistical methods: Pearson's, Spearman's, and Kendall's correlation coefficients. These coefficients characterize different types of dependence and robustness against nonlinearity and outliers. The Pearson correlation coefficient r measures the strength and direction of the linear relationship between two continuous variables x and y. It is defined as

$$r = \frac{\sum_{i=1}^{n}(x_i - \bar{x})(y_i - \bar{y})}{\sqrt{\sum_{i=1}^{n}(x_i - \bar{x})^2 \sum_{i=1}^{n}(y_i - \bar{y})^2}}, \tag{1}$$

where $\bar{x}$ and $\bar{y}$ are the sample means of the variables. The coefficient ranges between −1 and +1, representing perfect negative and perfect positive linear correlations, respectively. Statistical significance is evaluated using a two-tailed p-value (Rodgers & Nicewander 1988; Press et al. 1992).

The Spearman correlation coefficient ρ assesses the monotonic relationship between two variables based on ranked data. It is given by

$$\rho = 1 - \frac{6\sum d_i^2}{n(n^2 - 1)}, \tag{2}$$

where d_i is the difference between the ranks of corresponding values of x and y, and n is the sample size. Unlike Pearson's r, Spearman's ρ does not assume linearity or normality, making it suitable for non-parametric data (Isobe et al. 1990; Feigelson & Babu 2012).

The Kendall rank correlation coefficient τ evaluates the correspondence between the ordering of two variables. It is calculated as

$$\tau = \frac{N_c - N_d}{\frac{1}{2}n(n - 1)}, \tag{3}$$

where N_c and N_d are the numbers of concordant and discordant pairs, respectively. Kendall's τ is more robust for small datasets and when tied ranks occur (Wall & Jenkins 2003; Hollander et al. 2014).

All three correlation coefficients described above were applied to the newly compiled catalog of dwarf galaxies constructed in this study. For each pair of parameters, the Pearson (r), Spearman (ρ), and Kendall (τ) correlation coefficients were calculated to examine possible linear and monotonic relationships. The computations were performed using both MATLAB and Microsoft Excel software environments.

In MATLAB, the built-in statistical functions corr and corrcoef were employed to compute Pearson, Spearman, and Kendall correlations, along with their corresponding p-values. These tools provide flexible options for non-parametric and parametric analyses, ensuring numerical precision and reproducibility.

In Microsoft Excel, correlation coefficients were cross-verified using the CORREL and PEARSON functions, and rank-based coefficients were calculated using custom formulas for rank differences.

This dual approach allowed independent validation of the results and minimized computational bias. The resulting correlation matrix and regression equations revealed several statistically significant relationships among the catalog parameters.

2.2. Outlier Rejection

In order to minimize the possibility of gross errors (outliers), all measurements were organized in a way that prevents the appearance of accidental mistakes. According to the classical approach described by Agekyan (2014), a gross error should be regarded as an event with a probability close to zero. If such an error occurs, the corresponding measurement must be excluded from further analysis.

When a series of measurements includes one value that significantly deviates from the rest, this value can be treated as an outlier if it clearly does not correspond to the expected physical quantity. In such a case, the exclusion of the anomalous measurement is justified, especially when the reason for its occurrence can be identified. For a quantitative assessment, measurements that deviate considerably from the arithmetic mean of the series are recommended to be excluded. The exclusion criterion is expressed as

$$\frac{|x_i - \bar{x}|}{\sigma} > k, \tag{4}$$

where x_i is the individual measurement, $\bar{x}$ is the mean value of the remaining measurements, and σ is the standard deviation. For small datasets ($n \leqslant 6$), this statistical criterion is not recommended because the estimates of $\bar{x}$ and σ are unreliable. For larger samples ($n \geqslant 6$), a measurement is considered an outlier if the above condition is satisfied, with the coefficient k depending on the sample size as follows:

$$k = \begin{cases} 4, & \text{if } 6 < n \leqslant 100, \\ 4.5, & \text{if } 100 < n \leqslant 1000, \\ 5, & \text{if } n > 1000. \end{cases} \tag{5}$$

These threshold values ensure that the probability of erroneously rejecting a valid measurement remains very small (less than 0.00693). This method allows reliable identification and removal of gross errors without affecting the statistical integrity of the dataset. By applying this procedure, the measurement series used in this study was refined, and all values exceeding the established limit were excluded. As a result, the overall accuracy of the observational data and the reliability of the derived parameters were significantly improved.

2.3. Calculation of Regression Equations

The regression equations between the physical parameters of dwarf galaxies were derived using the least-squares method, which provides the best fit by minimizing the sum of squared deviations of the observed values from the theoretical model (Taylor 1997; Bevington & Robinson 2003).

For a set of paired data (x_i, y_i), the linear regression equation was determined in the form

$$y = a + bx, \tag{6}$$

where a is the intercept and b is the slope of the regression line. The coefficients were calculated using the standard least-squares formulas:

$$b = \frac{n\sum x_i y_i - \sum x_i \sum y_i}{n\sum x_i^2 - (\sum x_i)^2}, \tag{7}$$

$$a = \frac{\sum y_i - b\sum x_i}{n}. \tag{8}$$

In addition to the classical least-squares approach, the regression analysis was also performed within a Bayesian framework. This method allows for a probabilistic estimation of the regression parameters by incorporating measurement uncertainties and intrinsic scatter in the data.

For a set of paired data (x_i, y_i), the linear relation is expressed as

$$y = \alpha + \beta x, \tag{9}$$

where α is the intercept and β is the slope of the regression line. In the Bayesian approach, these parameters are treated as random variables and their posterior distributions are inferred from the data.

The likelihood function accounts for observational uncertainties in both variables as well as an additional intrinsic scatter term $\sigma_{\rm int}$, which represents the natural dispersion of the relation

$$y_i \sim \mathcal{N}(\alpha + \beta x_i, \quad \sigma_{\rm int}^2). \tag{10}$$

The regression parameters (α, β, and $\sigma_{\rm int}$) were estimated using a Markov Chain Monte Carlo method following the approach of Kelly (2007). This method provides robust parameter estimates and their uncertainties by sampling from the full posterior distribution.

All statistical calculations, including correlation coefficients and classical least-squares regressions, as well as graphical analyses, were performed using MATLAB R2024a and Microsoft Excel. The reliability of the obtained regression coefficients was verified using the standard deviation and Student's t-test at a 95% confidence level. In addition, Bayesian regression analyses were carried out in Python using the `linmix` implementation, which is designed to account for heteroscedastic measurement errors and intrinsic scatter in astronomical data.

3. Results

We present a catalog of 722 dwarf galaxies, each described by 18 parameters that characterize their positional, photometric, morphological, and kinematic properties. These parameters were collected and systematized from previously published observational data and publicly available astronomical databases. In particular, the core sample and several key physical parameters were compiled from the comprehensive review of nearby dwarf galaxies by McConnachie (2012) and supplemented with updated measurements from Kutlimuratov et al. (2019). Additional data were retrieved from major astronomical databases, including HyperLeda (Makarov et al. 2014), the NASA/IPAC Extragalactic Database (NED) (NASA/IPAC Extragalactic Database 2025), and the Database of the Local Volume Objects (Special Astrophysical Observatory of the Russian Academy of Sciences 2025). When multiple measurements were available for a given parameter, preference was given to the most recent and homogeneous sources, and all quantities were converted to a consistent system of units. For clarity and reproducibility, each parameter is briefly defined below, along with its physical meaning and the corresponding data sources. Based on the statistical analysis described in the previous section, several significant relationships between the studied parameters were identified.

Prior to the present study, the preliminary versions of this catalog and its underlying observational data were already employed in two peer-reviewed works. In the first study, empirical dependencies for irregular dwarf galaxies (Tillaboev et al. 2025b), the compiled data from the NASA/IPAC and HyperLeda databases were used to investigate empirical correlations among key physical parameters of irregular dwarf galaxies. A detailed statistical analysis revealed strong relationships between galaxy mass and distance, apparent stellar magnitude and distance, mass and absolute magnitude, as well as correlations involving redshift across different subclasses of irregular dwarf systems.

In a subsequent work, empirical dependencies for irregular and elliptical dwarf galaxies (Tillaboev & Tadjibaev 2025), an expanded version of the same catalog was applied to a comparative analysis of irregular (dIrr) and elliptical (dE) dwarf galaxies. Using regression and correlation techniques, this study identified strong negative correlations between absolute magnitude and galaxy mass, as well as strong positive correlations between galaxy mass, redshift, and surface brightness. Additionally, moderate correlations between dIrr and dE galaxies in terms of mass and luminosity were reported, providing further insight into the similarities and differences in their evolutionary properties.

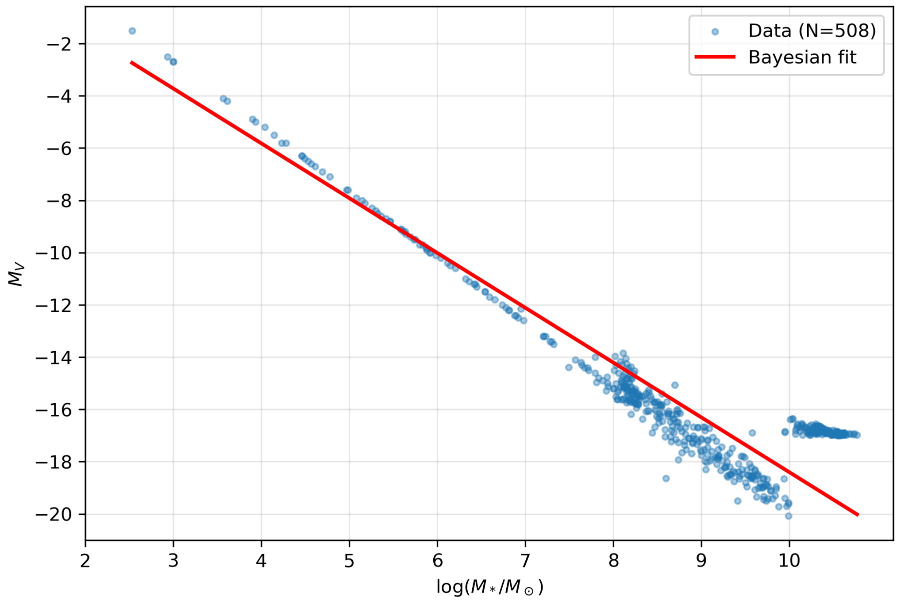

Figure 1. Bayesian linear regression between absolute magnitude (M_V) and stellar mass $\log(M_*/M_\odot)$ for the galaxy sample ($N = 508$).

These earlier studies demonstrated the reliability and scientific value of the catalog as a homogeneous dataset for statistical investigations of dwarf galaxy properties, thereby motivating its further expansion and refinement in the present work.

Absolute Magnitude of Galaxies and Stellar Mass (Figure 1): Strong negative correlations (Pearson = −0.90, Spearman = −0.76, Kendall = −0.62) indicate a robust inverse relationship between the absolute magnitude and the stellar mass of the galaxy. The classical regression relation is given by

$$M_V = -1.766\,(\pm 0.037)\,\log\left(\frac{M_*}{M_\odot}\right) - 0.203\,(\pm 0.329), \quad (11)$$

while the Bayesian linear regression yields

$$M_V = (-2.097 \pm 0.029)\,\log\left(\frac{M_*}{M_\odot}\right) + (2.570 \pm 0.240), \quad (12)$$

with an intrinsic scatter of $\sigma_{\rm int} = 0.275 \pm 0.078$.

Absolute Magnitude of Galaxies and Apparent Magnitude (Figure 2): The positive correlations (Pearson = 0.70, Spearman = 0.64, Kendall = 0.43) indicate a clear relationship between the apparent magnitude and the absolute magnitude of galaxies. The classical regression relation is given by

$$M_V = 0.769\,(\pm 0.038)\,m_r - 28.703\,(\pm 0.569), \quad (13)$$

while the Bayesian linear regression yields

$$M_V = (1.008 \pm 0.063)\,m_r + (-32.285 \pm 0.988), \quad (14)$$

with an intrinsic scatter of $\sigma_{\rm int} = 0.143 \pm 0.068$. Both approaches show a consistent positive relation between M_V and m_r, with the Bayesian model yielding a steeper slope.

Absolute Magnitude of Galaxies and Metallicity: The negative correlations (Pearson = −0.64, Spearman = −0.65, Kendall = −0.48, $N = 116$) indicate a clear inverse relationship between galaxy metallicity and absolute magnitude. The classical regression relation is given by

$$M_V = -4.420\,(\pm 0.495)\,[{\rm Fe/H}] - 17.961\,(\pm 0.859), \quad (15)$$

while the Bayesian linear regression yields

$$M_V = (-4.989 \pm 0.572)\,[{\rm Fe/H}] + (-19.023 \pm 0.986), \quad (16)$$

with an intrinsic scatter of $\sigma_{\rm int} = 2.473 \pm 0.192$. The Bayesian fit results in a steeper slope compared to the classical regression.

Absolute Magnitude of Galaxies and Central Surface Brightness (Figure 3): The positive correlations (Pearson = 0.58, Spearman = 0.61, Kendall = 0.45) indicate a moderate relationship between the absolute magnitude and the V-band surface brightness of galaxies. The classical regression relation is given by

$$M_V = 0.829\,(\pm 0.066)\,\mu_V - 32.505\,(\pm 1.585), \quad (17)$$

while the Bayesian linear regression yields

$$M_V = (0.974 \pm 0.082)\,\mu_V + (-35.869 \pm 1.950), \quad (18)$$

with an intrinsic scatter of $\sigma_{\rm int} = 2.307 \pm 0.114$. The Bayesian fit yields a steeper slope than the classical regression.

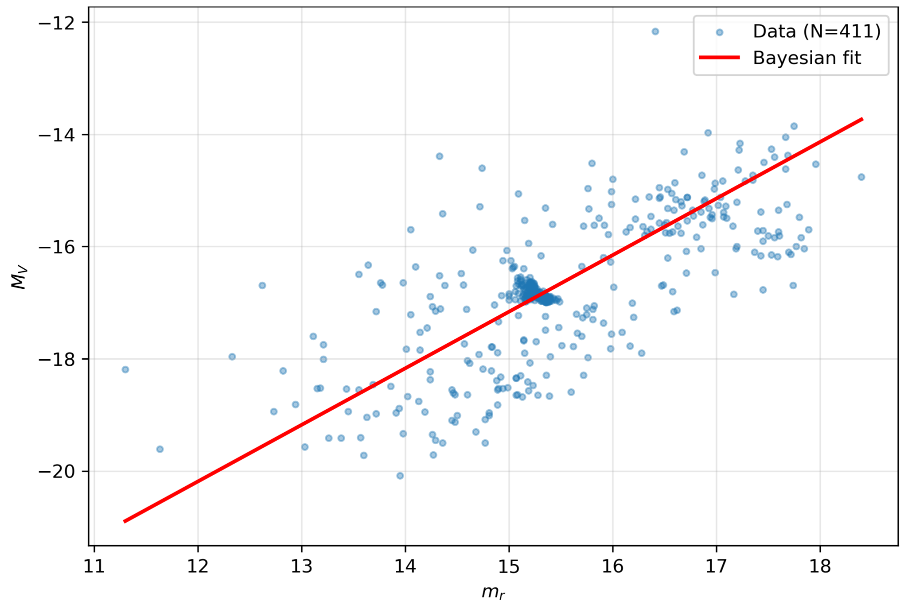

Figure 2. Bayesian linear regression between absolute magnitude (M_V) and apparent magnitude (m_r) for the galaxy sample (N = 411).

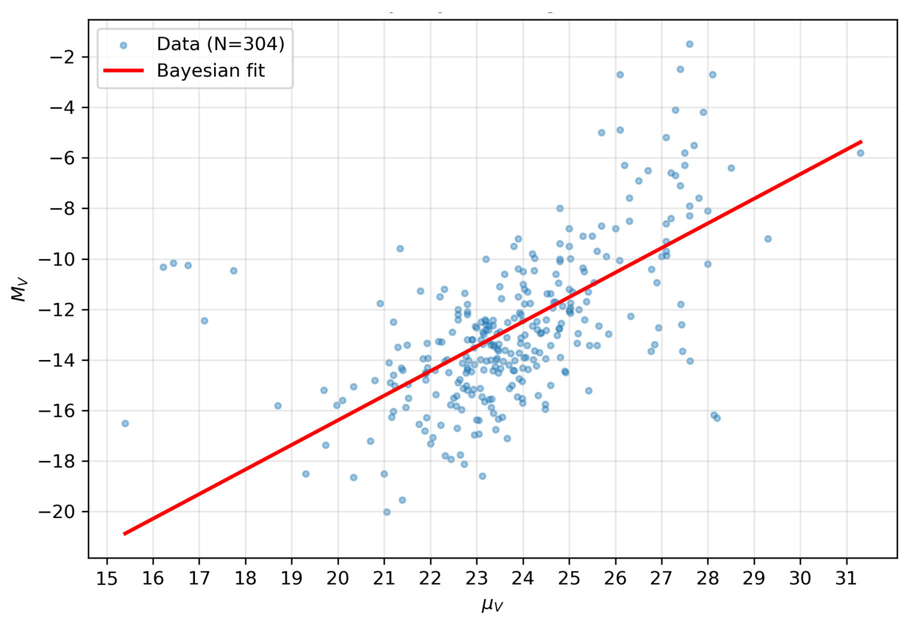

Figure 3. Bayesian linear regression between absolute magnitude (M_V) and central surface brightness (μ_V) for the galaxy sample (N = 304).

Absolute Magnitude of Galaxies and Logarithmic H I mass (Figure 4): The strong correlations (Pearson = −0.80, Spearman = −0.80, Kendall = −0.62) indicate a robust inverse relationship between the absolute magnitude and the logarithmic H I mass of galaxies. The classical regression relation is given by

$$M_V = -1.652\,(\pm 0.079)\log\left(\frac{M_{\rm HI}}{M_\odot}\right) - 1.616\,(\pm 0.568), \quad (19)$$

while the Bayesian linear regression yields

$$M_V = (-1.658 \pm 0.084)\log\left(\frac{M_{\rm HI}}{M_\odot}\right) + (-1.645 \pm 0.594), \quad (20)$$

with an intrinsic scatter of $\sigma_{\rm int} = 1.634 \pm 0.094$. The Bayesian fit is consistent with the classical regression, showing a similar slope within uncertainties.

Stellar Mass and Logarithmic H I mass: The strong positive correlations (Pearson = 0.82, Spearman = 0.77,

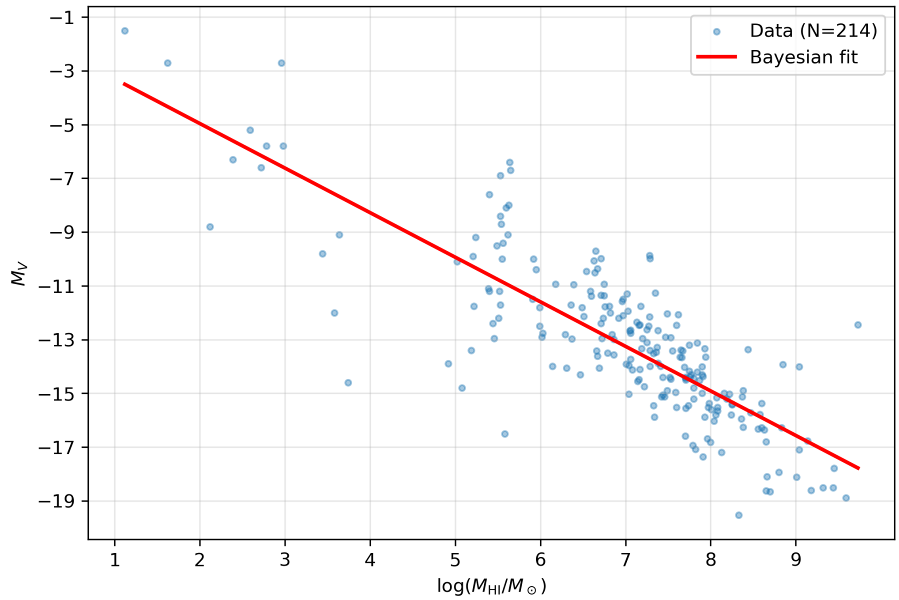

Figure 4. Bayesian linear regression between absolute magnitude (M_V) and logarithmic H I mass $\log(M_{\rm HI}/M_\odot)$ for the galaxy sample ($N = 214$).

Kendall = 0.60, $N = 68$) indicate a close relationship between the stellar mass of galaxies and their logarithmic H I mass. The classical regression relation is given by

$$\log\left(\frac{M_*}{M_\odot}\right) = (0.666 \pm 0.053) \times \log\left(\frac{M_{\rm HI}}{M_\odot}\right) + (2.541 \pm 0.337), \tag{21}$$

while the Bayesian linear regression yields

$$\log\left(\frac{M_*}{M_\odot}\right) = (0.674 \pm 0.058) \times \log\left(\frac{M_{\rm HI}}{M_\odot}\right) + (2.482 \pm 0.355), \tag{22}$$

with an intrinsic scatter of $\sigma_{\rm int} = 0.853 \pm 0.090$. The Bayesian fit is consistent with the classical regression, showing similar parameters within uncertainties.

Stellar Mass and Metallicity (Figure 5): The positive correlations (Pearson = 0.68, Spearman = 0.62, Kendall = 0.46) indicate a moderate relationship between galaxy stellar mass and metallicity. The classical regression relation is given by

$$\log\left(\frac{M_*}{M_\odot}\right) = (2.25 \pm 0.27)\,[\mathrm{Fe/H}] + (9.95 \pm 0.49), \tag{23}$$

while the Bayesian linear regression yields

$$\log\left(\frac{M_*}{M_\odot}\right) = (2.581 \pm 0.311)\,[\mathrm{Fe/H}] + (10.505 \pm 0.566), \tag{24}$$

with an intrinsic scatter of $\sigma_{\rm int} = 0.972 \pm 0.095$. The Bayesian fit yields a steeper slope compared to the classical regression.

Stellar Mass and Half-Light Radius: The positive correlations (Pearson = 0.55, Spearman = 0.67, Kendall = 0.49, $N = 90$) indicate a moderate relationship between galaxy stellar mass and half-light radius. The classical regression relation is given by

$$\log\left(\frac{M_*}{M_\odot}\right) = (1.66 \pm 0.29)\, r_h + (5.17 \pm 0.19), \tag{25}$$

while the Bayesian linear regression yields

$$\log\left(\frac{M_*}{M_\odot}\right) = (0.002 \pm 0.000)\, r_h + (5.093 \pm 0.198), \tag{26}$$

with an intrinsic scatter of $\sigma_{\rm int} = 1.161 \pm 0.097$. The Bayesian fit yields a significantly shallower slope compared to the classical regression.

Stellar Mass and Central Surface Brightness (Figure 6): The strong negative correlations (Pearson = −0.83, Spearman = −0.87, Kendall = −0.67) indicate a tight inverse relationship between galaxy stellar mass and V-band surface brightness. The classical regression relation is given by

$$\log\left(\frac{M_*}{M_\odot}\right) = -0.456\,(\pm 0.032)\,\mu_V + 17.25\,(\pm 0.79), \tag{27}$$

while the Bayesian linear regression yields

$$\log\left(\frac{M_*}{M_\odot}\right) = (-0.480 \pm 0.034)\,\mu_V + (17.800 \pm 0.857), \tag{28}$$

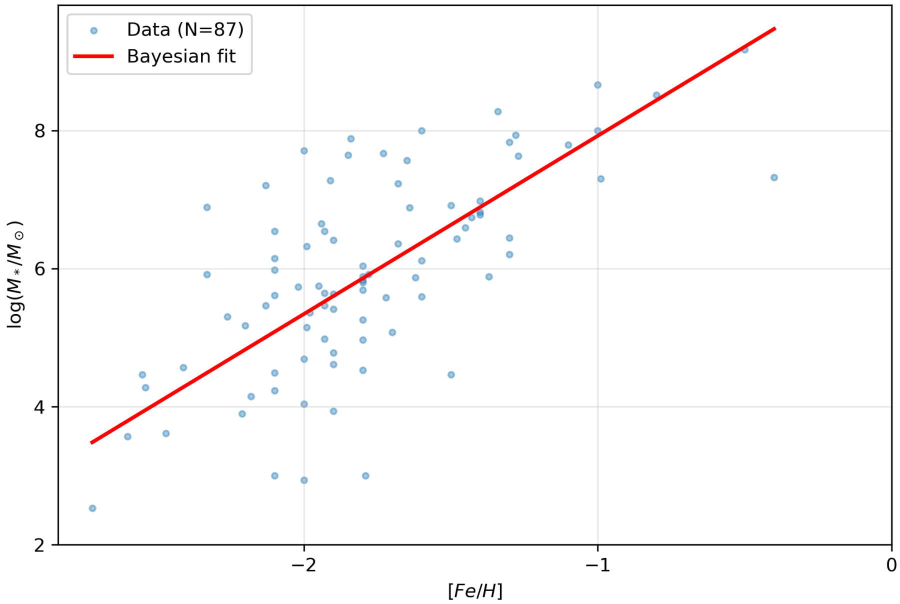

Figure 5. Relation between stellar mass $\log(M_*/M_\odot)$ and metallicity [Fe/H] obtained using Bayesian linear regression for 87 galaxies.

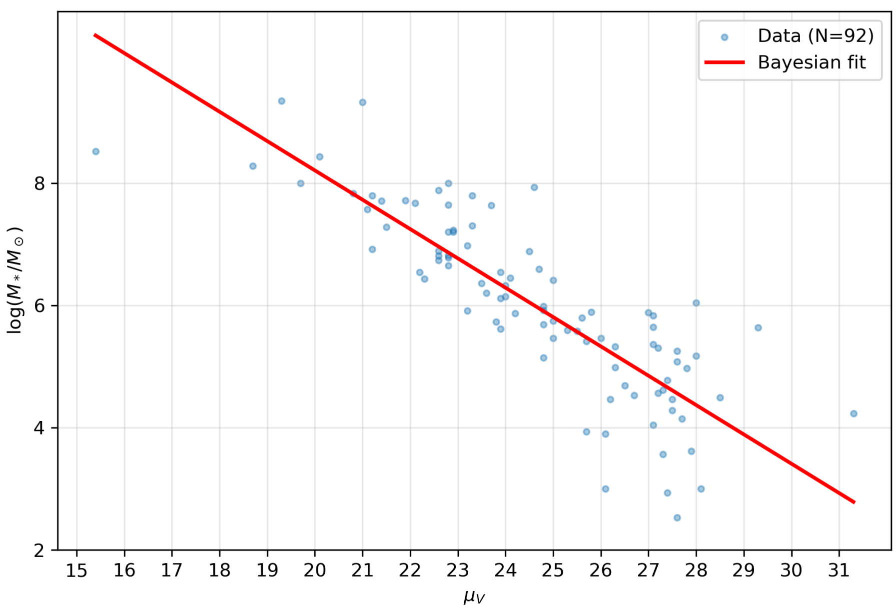

Figure 6. Bayesian linear regression between stellar mass $\log(M_*/M_\odot)$ and central surface brightness (μ_V) for the galaxy sample ($N = 92$).

with an intrinsic scatter of $\sigma_{\rm int} = 0.722 \pm 0.073$. The Bayesian fit is consistent with the classical regression, showing similar parameters within uncertainties.

Metallicity and Central Surface Brightness (Figure 7): The negative correlations (Pearson $= -0.62$, Spearman $= -0.52$, Kendall $= -0.37$) indicate a moderate inverse relationship between metallicity and V-band surface brightness. The classical regression relation is given by

$$[{\rm Fe/H}] = -0.102\,(\pm 0.012)\,\mu_V + 0.812\,(\pm 0.302), \quad (29)$$

while the Bayesian linear regression yields

$$[{\rm Fe/H}] = (-0.111 \pm 0.014)\,\mu_V + (1.010 \pm 0.346), \quad (30)$$

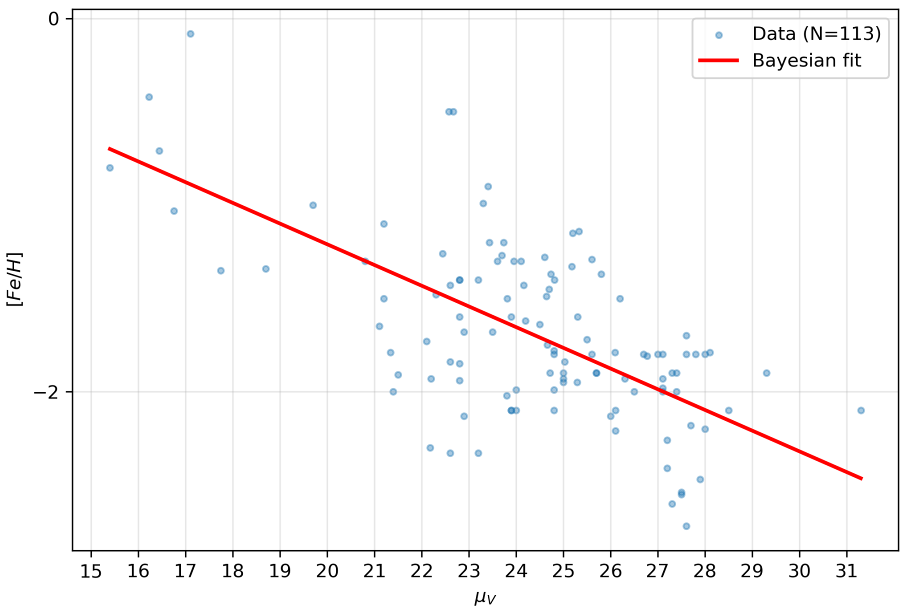

Figure 7. Bayesian linear regression between metallicity [Fe/H] and central surface brightness (μ_V) for the galaxy sample ($N = 113$).

with an intrinsic scatter of $\sigma_{\rm int} = 0.336 \pm 0.030$. The Bayesian fit is consistent with the classical regression, showing similar parameters within uncertainties.

4. Discussion

The novelty of this study lies in the identification of statistically significant Spearman and Kendall rank correlations among the physical parameters of dwarf galaxies. Relationships between galaxy properties are often nonlinear, highly scattered, and affected by measurement uncertainties and selection effects, particularly in low-mass systems. In addition to this, the derived regression relations enable a direct comparison between classical least-squares and Bayesian approaches, allowing a deeper physical interpretation of the observed scaling relations. By relying on relative rankings rather than absolute values, Spearman's ρ and Kendall's τ are less sensitive to outliers and heterogeneous uncertainties, making them well suited for the analysis of dwarf galaxy samples (Isobe et al. 1990; Conover 1999; Feigelson & Babu 2012).

A systematic difference is observed between classical and Bayesian regressions. In several relations (e.g., M_V–$\log(M_*/M_\odot)$, M_V–[Fe/H], M_V–μ_V, $\log(M_*/M_\odot)$–[Fe/H]), the Bayesian method yields steeper slopes, whereas in others (e.g., $\log(M_*/M_\odot)$–$\log(M_{\rm HI}/M_\odot)$ and $\log(M_*/M_\odot)$–μ_V) both approaches produce nearly identical results. This indicates that Bayesian regression reveals stronger intrinsic dependencies when observational uncertainties and intrinsic scatter are properly accounted for.

The strong negative correlation confirms that stellar mass is the primary driver of galaxy luminosity. The steeper Bayesian slope (-2.097 versus -1.766) suggests that classical regression underestimates the strength of this relation due to unaccounted scatter in low-mass systems. This implies that star formation efficiency is more tightly regulated by halo mass than inferred from classical models.

For the M_V–m_r relation, the Bayesian slope is significantly steeper, indicating that observational uncertainties (e.g., distance effects) flatten the classical relation. Similarly, the M_V–μ_V relation shows a steeper Bayesian slope, suggesting that central surface brightness is more strongly connected to galaxy luminosity and stellar density. In contrast, the M_V–$\log(M_{\rm HI}/M_\odot)$ relation shows nearly identical slopes in both methods, indicating that neutral hydrogen mass is a robust tracer of galaxy luminosity and is less affected by observational uncertainties.

M_V–[Fe/H] and $\log(M_*/M_\odot)$–[Fe/H] relations show systematically steeper slopes in the Bayesian framework, indicating that chemical enrichment is more strongly dependent on galaxy mass than suggested by classical regression. This supports the physical scenario in which more massive dwarf galaxies retain metals more efficiently, while low-mass systems lose metals through stellar feedback-driven outflows. The relatively large intrinsic scatter confirms that metallicity is influenced by additional processes such as star formation history and environmental effects.

The $\log(M_*/M_\odot)$–$\log(M_{\rm HI}/M_\odot)$ relation shows excellent agreement between classical and Bayesian slopes, indicating a fundamental coupling between gas content and stellar mass. Similarly, the $\log(M_*/M_\odot)$–μ_V relation is consistent in both methods, suggesting that surface brightness is a stable structural indicator of stellar mass. In contrast, the $\log(M_*/M_\odot)$–r_h relation exhibits a significant discrepancy: the Bayesian slope is close to zero, while the classical regression predicts a strong dependence. This suggests that the apparent size–mass relation in classical analysis may be driven by scatter or selection effects rather than a true physical correlation.

Both methods yield consistent slopes, indicating a reliable inverse relation between metallicity and surface brightness. This implies that low surface brightness galaxies are typically metal-poor, consistent with inefficient star formation and enhanced gas loss.

Previous studies, such as McConnachie (2012), focused primarily on dwarf galaxies within and around the Local Group, where environmental effects from massive host galaxies dominate. In contrast, the present work extends the analysis to a compiled catalog reaching distances of $\sim$121 Mpc, thereby probing a much broader range of cosmic environments. The persistence of statistically significant correlations across this extended volume indicates that the identified trends are not unique to the Local Group but instead reflect more general properties of dwarf galaxies.

Although Kutlimuratov et al. (2019) constructed a valuable catalog of dwarf galaxies out to similar distances, their analysis remained largely descriptive. Our study goes beyond this work by placing the observed relations within a robust statistical and physical framework. In particular, we explicitly distinguish between correlations driven by observational selection effects and those that trace intrinsic physical processes.

In contrast, correlations among intrinsic galaxy properties, such as mass, luminosity, metallicity, surface brightness, and size, provide insight into the physical mechanisms governing dwarf galaxy formation and evolution. The strong anti-correlation between absolute magnitude and galaxy mass, further reinforced by the steeper slope obtained in the Bayesian regression, suggests that luminosity remains more tightly coupled to the depth of the gravitational potential than inferred from classical methods. This behavior is consistent with ΛCDM-based models, in which more massive dark matter haloes are able to convert a larger fraction of baryons into stars.

The steeper Bayesian slope indicates that more massive dwarf galaxies are even more efficient at retaining metals against stellar feedback-driven outflows than suggested by classical regression. In shallow potential wells, stellar winds and supernova feedback can readily expel metal-enriched gas, whereas deeper haloes suppress large-scale outflows and enable sustained chemical enrichment. The relatively large intrinsic scatter obtained in the Bayesian analysis further indicates that metallicity is influenced by additional processes such as star formation history and environmental effects. This interpretation is well established both observationally and theoretically (Reaves 1983). The observed scatter in these relations likely reflects variations in star formation histories, gas accretion, and environmental influence.

Additional support comes from the inverse correlation between metallicity and surface brightness. The consistency between classical and Bayesian slopes in this relation suggests that it represents a robust physical connection rather than an artifact of observational uncertainties. Low-surface-brightness dwarf galaxies tend to be metal-poor, consistent with inefficient star formation and enhanced metal loss, while higher-surface-brightness systems appear to have retained gas and metals more effectively, allowing prolonged star formation and chemical enrichment (Reaves 1983).

Despite the relatively large sample size, several limitations remain. The compiled catalog is heterogeneous, combining measurements from different surveys with varying methodologies and calibrations. Systematic uncertainties in distance estimates, mass determinations, and metallicity measurements contribute to the observed scatter; however, the Bayesian framework allows this intrinsic scatter to be explicitly quantified. The agreement between classical and Bayesian results in several relations confirms that the main scaling relations are physically robust, while discrepancies highlight cases where observational uncertainties play a significant role.

Overall, the comparison between classical and Bayesian regression reveals that some scaling relations are significantly affected by observational uncertainties, leading to underestimated slopes in classical analysis. Bayesian regression corrects for these effects and provides a more accurate representation of the underlying physical processes. The results confirm that galaxy mass is the dominant parameter governing luminosity, metallicity, and gas content, while structural parameters such as size may exhibit weaker or more complex dependencies. These findings are consistent with ΛCDM-based models, in which the dark matter halo mass regulates star formation efficiency, gas retention, and chemical enrichment in dwarf galaxies.

5. Conclusions

This research investigates the broad parameter space of dwarf galaxies and combines classical and Bayesian regression analyses to identify the most reliable indicators of the physical processes that drive low-mass galaxy evolution. By assembling a large and diverse sample, we were able to assess the relative importance of different observables without relying on assumptions specific to individual subsamples or environments.

A key outcome of this analysis is the identification of galaxy mass as the dominant organizing parameter of dwarf galaxy properties, consistently confirmed by both classical and Bayesian regression results. The persistence of tight relations among intrinsic quantities, together with the steeper slopes obtained in Bayesian fits for several key relations, indicates that the internal structure of dwarf galaxies is more strongly regulated by the depth of their gravitational potential wells than inferred from classical methods. This result reinforces the view that dark matter halo mass sets the fundamental boundary conditions for baryonic evolution in low-mass systems. Our findings further suggest that surface brightness and metallicity act as sensitive tracers of baryonic processing within dwarf galaxies, with Bayesian regression indicating stronger dependencies in these relations. Low surface brightness and metal-poor systems appear to occupy a regime where stellar feedback efficiently redistributes or removes gas, suppressing sustained star formation and chemical enrichment. The relatively large intrinsic scatter observed in metallicity-related relations reflects the complex interplay between star formation history, gas accretion, and environmental effects.

A central result of this work is the systematic difference between classical and Bayesian regression. In several relations, the Bayesian method yields steeper slopes, indicating that classical regression tends to underestimate the strength of physical dependencies due to unaccounted measurement uncertainties and intrinsic scatter. At the same time, the agreement between the two methods in relations such as stellar mass–H I mass and stellar mass–surface brightness demonstrates that some scaling relations are intrinsically robust and only weakly affected by observational uncertainties.

Importantly, the empirical relations reported here, particularly when interpreted within the Bayesian framework, are not merely descriptive but provide quantitative constraints on the range of viable galaxy formation scenarios. Any successful theoretical or numerical model operating within the ΛCDM framework must simultaneously reproduce the observed scaling relations among mass, luminosity, gas content, metallicity, and structural parameters in the dwarf regime. Deviations from these relations may signal variations in feedback efficiency, environmental influence, or departures from standard assumptions about dark matter–baryon coupling. In this sense, dwarf galaxies emerge as critical laboratories for testing galaxy formation physics on the smallest scales accessible to current observations. The statistically robust trends identified in this work establish a benchmark against which future homogeneous surveys and high-resolution cosmological simulations can be compared, particularly in the context of testing the role of feedback, gas retention, and dark matter–baryon coupling in low-mass galaxies.

Acknowledgments

The authors are grateful to professor S.N. Nuritdinov for posing the problems and discussing the results.

Data Availability

This research made use of publicly available data from major astronomical databases, including HyperLeda, the NASA/IPAC Extragalactic Database (NED), and the Database of the Local Volume Objects. The compiled dataset generated during this study is available from the corresponding author upon reasonable request.

ORCID iDs

K. Tillaboev https://orcid.org/0000-0002-9299-1854

References

Agekyan, T. A. 2014, Fundamentals of Error Theory for Astronomers and Physicists (2nd ed.; Nauka)
Ahvazi, N., Benson, A., Sales, L. V., et al. 2024, MNRAS, 529, 3387
Annibali, F., & Tosi, M. 2022, NatAs, 6, 48
Atek, H. 2018, Proceedings of the International Astronomical Union, 14, 429
Battaglia, G., Helmi, A., Tolstoy, E., et al. 2008, ApJL, 681, L13
Behroozi, P. S., Wechsler, R. H., & Conroy, C. 2012, ApJL, 762, L31
Bevington, P. R., & Robinson, D. K. 2003, Data Reduction and Error Analysis for the Physical Sciences (3rd ed.; McGraw-Hill)
Boldrini, P. 2022, Galaxies, 10, 5
Boylan-Kolchin, M., Bullock, J. S., & Kaplinghat, M. 2011, MNRAS: Letters, 415, L40
Brown, T. M., Tumlinson, J., Geha, M., et al. 2014, ApJ, 796, 91
Bullock, J. S., & Boylan-Kolchin, M. 2017, ARA&A, 55, 343
Caldwell, N. 1987, AJ, 94, 1116
Chauhan, R., Subramanian, S., Kudari, D. A., Amrutha, S., & Das, M. 2025, A&A, 702, A222
Conover, W. J. 1999, Practical Nonparametric Statistics (3rd ed.; Wiley)
de Blok, W. J. G. 2010, AdAst, 2010, 789293
Feigelson, E. D., & Babu, G. J. 2012, Modern Statistical Methods for Astronomy: With R Applications (Cambridge Univ. Press)
Frebel, A., & Norris, J. E. 2015, ARA&A, 53, 631
Garrison-Kimmel, S., Wetzel, A., Hopkins, P. F., et al. 2019, MNRAS, 489, 4574
Governato, F., Brook, C., Mayer, L., et al. 2010, Natur, 463, 203
Hollander, M., Wolfe, D. A., & Chicken, E. 2014, Nonparametric Statistical Methods (3rd ed.; Wiley)
Isobe, T., Feigelson, E. D., Akritas, M. G., & Babu, G. J. 1990, ApJ, 364, 104
Janz, J., Salo, H., Su, A. H., & Venhola, A. 2021, A&A, 647, A80
Johnston, K. V., Zhao, H., Spergel, D. N., & Hernquist, L. 1999, ApJL, 512, L109
Karachentsev, I. D., & Kaisina, E. I. 2019, AstBu, 74, 111
Kelly, B. C. 2007, ApJ, 665, 1489
Kirby, E. N., Cohen, J. G., Guhathakurta, P., et al. 2013, ApJ, 779, 102
Klypin, A., Kravtsov, A. V., Valenzuela, O., & Prada, F. 1999, ApJ, 522, 82
Koudmani, S., Rennehan, D., Somerville, R. S., et al. 2025, MNRAS, 540, 1928
Kutlimuratov, S., Tadjibaev, I., & Nuritdinov, S. 2019, Uzbek Journal of Physics, 22, 203
Leitner, S. N. 2012, ApJ, 745, 149
Makarov, D., Prugniel, P., Terekhova, N., Courtois, H., & Vauglin, I. 2014, A&A, 570, A13
Mateo, M. 1998, ARA&A, 36, 435
McConnachie, A. W. 2012, AJ, 144, 4
NASA/IPAC Extragalactic Database 2025, NASA/IPAC Extragalactic Database (NED), https://ned.ipac.caltech.edu/, accessed: 2026-02-18
Navarro, J. F., Frenk, C. S., & White, S. D. M. 1996, ApJ, 462, 563
Pontzen, A., & Governato, F. 2012, MNRAS, 421, 3464
Press, W. H., Teukolsky, S. A., Vetterling, W. T., & Flannery, B. P. 1992, Numerical Recipes in C. The Art of Scientific Computing (2nd ed.; Cambridge Univ. Press)
Read, J. I., Iorio, G., Agertz, O., & Fraternali, F. 2017, MNRAS, 467, 2019

Reaves, G. 1983, ApJS, 53, 375
Rodgers, J., & Nicewander, W. 1988, Am. Stat., 42, 59
Sanati, M., Jeanquartier, F., Revaz, Y., & Jablonka, P. 2023, A&A, 669, A94
Saviane, I., Held, E. V., & Bertelli, G. 2000, A&A, 355, 56
Special Astrophysical Observatory of the Russian Academy of Sciences 2025, Local Volume Galaxy Database (LVGDB), https://www.sao.ru/lv/lvgdb/, accessed: 2026-02-18
Springel, V., White, S. D. M., Jenkins, A., et al. 2005, Natur, 435, 629
Straight, M. C., Boylan-Kolchin, M., Bullock, J. S., et al. 2025, MNRAS, 543, 1995
Taylor, J. R. 1997, An Introduction to Error Analysis: The Study of Uncertainties in Physical Measurements (2nd ed.; Univ. Science Books)
Tillaboev, K., Tadjibaev, I., Mamadaliyev, K., et al. 2025a, Galaxies, 13, 117
Tillaboev, K., Tadjibaev, I., & Otojanova, N. 2025b, A&AT, 35, 245
Tillaboev, K. T., & Tadjibaev, I. U. 2025, MUPB, 80, S303
van den Bergh, S. 1959, PDDO, 2, 147
Vogelsberger, M., Zavala, J., & Loeb, A. 2012, MNRAS, 423, 3740
Vogelsberger, M., Zavala, J., Simpson, C., & Jenkins, A. 2014, MNRAS, 444, 3684
Wall, J. V., & Jenkins, C. R. 2003, Practical Statistics for Astronomers, Cambridge Observing Handbooks for Research Astronomers (Cambridge Univ. Press)
Weisz, D. R., Dolphin, A. E., Skillman, E. D., et al. 2014, ApJ, 789, 147
Wheeler, C., Oñorbe, J., Bullock, J. S., et al. 2015, MNRAS, 453, 1305
White, S. D. M., & Rees, M. J. 1978, MNRAS, 183, 341
Wise, J. 2016, Uncovering the Origin and Evolution of Dwarf Galaxies, NSF Award Number 1614333, Directorate for Mathematical and Physical Sciences, Division Of Astronomical Sciences
Zimmermann, T., Alvey, J., Marsh, D. J. E., Fairbairn, M., & Read, J. I. 2025, PhRvL, 134, 151001